

# An Algorithm for Real-time Vessel Enhancement and Detection

Riccardo Poli  
School of Computer Science  
The University of Birmingham  
United Kingdom

and

Guido Valli  
Department of Electronic Engineering  
University of Florence  
Italy

## Abstract

In this paper we present a algorithm for the real-time enhancement and detection of blood vessels in medical images. The algorithm is based on a set of linear filters sensitive to vessels of different orientation and thickness. Such filters are obtained as linear combinations of properly shifted Gaussian kernels. The output of multiple oriented vessel-enhancing filters can be integrated to obtain images in which vessels are highly enhanced independently of their direction and thickness. To avoid spurious responses in the presence of step edges or to enhance the skeletons of vessels, the output of directional filters can be validated before integration. Skeleton detection and vessel segmentation can be performed via thresholding with hysteresis. Experimental results on synthetic images and real coronary arteriograms are reported.

## Keywords

Vessel Enhancement, Vessel Detection, Realtime Processing,  
Skeleton Detection, Vessel Segmentation.

## Address for Correspondence

Riccardo Poli  
School of Computer Science  
The University of Birmingham  
Edgbaston  
Birmingham B15 2TT  
United Kingdom  
E-mail: R.Poli@cs.bham.ac.uk  
Phone: +44-121-414-3739

# 1 Introduction

The quantitative, computer-based assessment of the characteristics and functionality of blood vessels in medical images plays an important role in clinical and research studies on a number of diseases. Many measurements can be performed off-line using graphical environments and accurate user-driven estimation algorithms, once the images have been acquired and stored.

The starting point for this kind of analyses is often the detection of the vessels in an image. Despite some aids, when the number of vessels of interest is large and/or their detection in a large number of (e.g. time-varying) images is required, this task can be extremely lengthy and tedious. For this reason the problem of computer-based vessel detection has been addressed with several classes of methods during the past two decades. Unfortunately, the presence of noise, the variability of the background and the low and varying contrast of vessels in many imaging modalities make it quite difficult to obtain reliable automatic or semi-automatic vessel detection algorithms.

In the following section we give a summary of the approaches used to overcome these difficulties and the problems encountered with them. Then, in Section 3, we discuss the success criteria of such approaches and propose a different set of objectives. The vessel enhancement and detection algorithm obtained by trying to reach these objectives is described in Section 4. In Sections 5 and 6 we report on some experiments with the algorithm and in Section 7 we make some final remarks.

## 2 Background

One of the most frequently investigated techniques for vessel detection is *vessel tracking* [1, 16, 22, 23, 24, 25, 27, 34]. Given a starting point and direction of a vessel, vessel tracking usually consists in sequentially locating other points belonging to the boundary of the vessel by analysing the gray levels of the pixels on a line-segment orthogonal to the tracking direction. Based on a more sophisticated version of the tracking idea are the methods that map the problem of detecting vessel boundaries to that of finding the optimum path in a graph [15, 18, 31]. In many cases these two classes of methods achieve rather good reliability. They are able to do so by drastically reducing the search space through the exploitation of *a priori* knowledge on the position of one or more reference points belonging to vessels and basic anatomical knowledge on the elongated cylinder-like shape of vessels. The disadvantage of these methods is that they are not fully automated.

Other classes of methods based on artificial intelligence or computer vision techniques have been proposed to obtain complete automation of the detection procedure [6, 9, 12, 28, 29, 33, 36, 39, 37]. Basically, although in different ways, all of them try to achieve this objective by extensively exploiting anatomical knowledge. In terms of accuracy, sensitivity and specificity these methods offer quite reasonable performance levels. Unfortunately, the complexity of the operations they perform to locate the vessels and (in some systems) to recognise them imposes computation times much larger than those required by the best tracking methods which, in turn, can be orders of magnitude bigger than those required for real-time processing.

Most of the above-mentioned methods adopt edge detection as a main tool for vessel detection. As vessel boundaries are usually smooth and fuzzy and the background is noisy, some authors have considered the strategy of trying to enhance vessels as much as possible before applying any detection procedures. This enhancement stage can offer two

advantages: a) it can increase the sensitivity of the detection algorithms applied after it, b) it can speed up the search as fewer non-vessels can “distract” the detection algorithms.

A first kind of approach to vessel enhancement is based on multiple rotation-invariant or linear morphological operators of proper sizes and orientations which are applied to the image to remove background and noise [30, 35, 38]. An advantage of such operators is their high selectivity to gray-level patterns similar to the structuring element(s) adopted; a disadvantage is that they are usually remarkably computation demanding.

An alternative approach is based on the convolution of the image with multiple matched filters, each one designed to detect vessels of a given width and orientation [2, 3, 4, 10, 20]. Matched filtering has shown a selectivity like that of morphological operators, but as the convolution kernels for each scale and orientation are usually large, it also shares the same high computation load.

### 3 Objectives

The focus of the research summarised in the previous section has been quality: both in terms of specificity and of sensitivity. The result is that enhancement and detection techniques are now available which can overcome the detection problems due, for example, to the image noise and the background inhomogeneity, and can be used to build reliable automatic systems. Unfortunately, in most cases, the complexity of the task has forced researchers not to try and balance the quality of the results with the efficiency with which they are obtained, but to seek the maximum quality (nearly) at any cost. However, when the number of images to be processed is very large and/or the algorithm has to work on-line in real-time (e.g. in a video-angiographic chain), different quality vs. efficiency trade-offs are needed.<sup>1</sup>

The objective of the work described in this paper was to try and develop an algorithm for blood-vessel enhancement in medical images with the highest possible performance both in terms of quality of results and of number of operations per pixel with the strict requirement of keeping the algorithm as close as possible to real-time processing. The motivation was that an algorithm with these features could then be used not only to improve the performance of any of the detection techniques described above without adding significantly to the computation they require, but also, in conjunction with simpler detectors, to obtain realtime or near-realtime vessel detection and segmentation.

### 4 Algorithm

As a first approximation vessels can be considered bar-like structures in the image. Therefore, for any given direction and width, they can be enhanced using convolution masks having a bar-like positive area surrounded by a negative neighbourhood which suppresses the output in the presence of a constant background. A schematic version of one such masks is shown on the left of Figure 1.

Our enhancement algorithm is based on linear operators of this kind which are convolved with the image to be enhanced. In this the algorithm does not differ significantly from other matched-filter-based enhancement algorithms. The distinctive feature of our algorithm is that in all the steps of the design of the convolution masks and of other

---

<sup>1</sup>We use the term *realtime processing* to mean that hardware and software are able to process at least 10 images per second, a rate that can still give a human observer the illusion of continuity of motion.

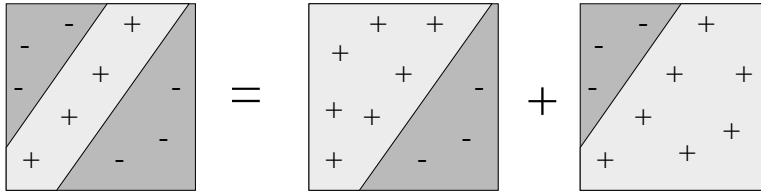


Figure 1: Decomposition strategy used to build efficient vessel-enhancing convolution masks.

parts of the algorithm extreme care has been taken to obtain maximum efficiency. The result is an algorithm that can operate in real-time on a modern workstation without any specialised hardware. Another characteristic of the algorithm is that the output of the operators sensitive to vessels of different orientation and scale is integrated and validated to prevent the enhancement of image structures not representing vessels.

The design of the algorithm is based on the following ideas.

## 4.1 Strategy

Firstly, it is important to recall that convolution is a linear operation, i.e.

$$I(\mathbf{x}) * (\lambda_1 M_1(\mathbf{x}) + \lambda_2 M_2(\mathbf{x})) = \lambda_1 I(\mathbf{x}) * M_1(\mathbf{x}) + \lambda_2 I(\mathbf{x}) * M_2(\mathbf{x}),$$

where  $I(\mathbf{x})$  denotes the gray level of the pixel of position  $\mathbf{x} = [x_1, x_2]$  of the input image,  $*$  is the convolution operator,  $M_i(\mathbf{x})$  ( $i = 1, 2$ ) are two convolution masks and  $\lambda_i$  ( $i = 1, 2$ ) are arbitrary coefficients. This means that if a mask can be expressed as a linear combination of two or more masks, then the convolution of an image with such a mask can be computed by linearly combining the images resulting from the convolution of the original image with each of the component masks.

Bar-like masks like the one depicted on the left of Figure 1 can often be constructed by combining (adding) two properly shifted and rotated step-like masks as indicated on the right of Figure 1. Therefore, convolving an image with a bar-like decomposable mask is equivalent to convolve the image with two step-like masks and then adding the results.

This top-down process of decomposing one mask into simpler ones is general and can be applied recursively for several times until non-decomposable convolution masks are obtained. If the “atomic” masks are extremely simple and the various compositions can be performed efficiently, the convolution of the image with the original bar-like masks can be performed very efficiently too (by convolving the image with the atomic masks and then appropriately combining the resulting images). However, if such masks are large or the composition is complex this top-down approach can result in a small efficiency gain.

An alternative approach to filter design is to start from very efficient atomic masks and try and combine them in efficient ways to obtain a filter that approximates the desired one (e.g. a directional vessel-enhancing mask). This bottom-up approach guarantees efficiency, but it does not offer total control on the degree of approximation obtained.

In designing our vessel-enhancing algorithm we have used a mixture of the aforementioned approaches. To design vessel-enhancing masks we have combined, in a bottom-up fashion, large (and therefore theoretically inefficient) Gaussian kernels, which offer very good approximation properties. To regain efficiency, a top-down approach has been used to decompose such kernels by means of two, very efficient, atomic masks (which compute the sum of two consecutive pixels in a row and in a column of the image, respectively).

The net result of this strategy is a complete, very efficient and accurate decomposition of large bar-like masks in term of tiny atomic masks.

The following sub-sections explain the strategy in detail. Gaussian filtering and the decomposition of Gaussian masks is described in Sections 4.2. Section 4.3 illustrates how such primitives can be used to build directional derivative estimation filters (a form of step-edge detectors) which are then combined (Section 4.4) to build directional vessel-enhancement filters. Then we show how the output of these filters can be integrated and validated to enhance vessels independently of their direction and width, as reported in Section 4.5. As all these steps are performed very efficiently the resulting enhancement algorithm works in real-time and can be integrated with a simple hysteresis-thresholding algorithm to obtain very efficient skeleton detection and vessel segmentation as detailed in Section 4.6.

## 4.2 Gaussian Smoothing

In our method Gaussian masks are used in a bottom-up fashion as building blocks to construct directional vessel-enhancing masks. The convolution of the image  $I(\mathbf{x})$  with a Gaussian kernel<sup>2</sup>

$$G(\mathbf{x}) = \exp\left(-\frac{x_1^2 + x_2^2}{2\sigma^2}\right),$$

produces a smoothed, noise-cleaned image

$$S(\mathbf{x}) = G(\mathbf{x}) * I(\mathbf{x}).$$

If performed as a two-dimensional convolution, the above calculation can be quite demanding (expecially for large values of  $\sigma$ ). So, even if the construction of vessel-enhancing masks is very efficient (see below), the computation of  $S(\mathbf{x})$  would make the algorithm inefficient. Fortunately, several strategies can be used to regain efficiency.

Firstly, it is worth noting that Gaussian kernels are separable [8, 11], i.e. they can be expressed as  $G(\mathbf{x}) = g(x_1)g(x_2)$  with  $g(z) = \exp\left(-\frac{z^2}{2\sigma^2}\right)$ . This means that the two-dimensional convolution  $G(\mathbf{x}) * I(\mathbf{x})$  can be performed efficiently by convolving the 1-D kernel  $g(z)$  with the columns of the image resulting from the convolution of the rows of  $I(\mathbf{x})$  with the same kernel, i.e.

$$S(\mathbf{x}) = (g(x_1) * I(x_1, x_2)) * g(x_2).$$

Usually, when the one-dimensional convolution is implemented with finite impulse response filters, the mask for convolution is obtained by sampling  $g(z)$  and neglecting the samples for which  $g(z) \approx 0$  (e.g. for  $|z| > 4\sigma$ ). However, even exploiting the separability of Gaussian masks and neglecting the “tails” can be insufficient to give realtime performance.

Fortunately, the following binomial approximation for one-dimensional Gaussian kernels exists:

$$g(z) \approx \frac{\sqrt{2\pi}\sigma}{2^{4\sigma^2}} \binom{4\sigma^2}{z + 2\sigma^2}$$

which, for small values of  $\sigma$ , is extremely convenient. This equation, valid when  $2\sigma^2$  and  $z$  are integers, can be derived with simple calculations from the Central Limit Theorem [32]. The approximation is good for  $\sigma$  as small as 1 (RMSE=0.033).

---

<sup>2</sup>For the sake of simplicity, but without loss of generality, in this paper we will disregard the normalisation factor of Gaussian kernels.

The considerable advantage of using binomial kernels is that they can be decomposed as sequences of successive convolutions with uniform kernels. Actually, the 1-D convolution with a binomial kernel can be obtained, in integer arithmetics, by successively computing for  $4\sigma^2$  times the convolution with an atomic kernel which returns the sum of two consecutive pixels, followed by a normalisation with a number power of two [5, 8, 13]. So, disregarding the normalisation factor,

$$I(z) * g(z) \approx (\cdots ((I(z) * \underbrace{u(z) * u(z)}_{4\sigma^2 \text{ times}}) * \cdots) * u(z))$$

where  $I(z)$  is a row or a column of  $I(\mathbf{x})$  and  $u(z)$  is the mask  $[1 \ 1]$  (i.e.  $I(z) * u(z) = I(z) + I(z + 1)$ ).

By using all the speed-up techniques mentioned above we can perform 2-D Gaussian smoothing with  $8 \times \sigma^2$  integer additions followed by a normalisation (a bit shift) only.

### 4.3 Directional Derivative Estimation

Once an efficient decomposition of  $G(\mathbf{x})$  is available, we can start using  $G(\mathbf{x})$  to build other masks capable of emphasising vessels or some of their features. As tracts of vessels can be approximately thought of as pairs of close, parallel step-edges with opposite contrast, we start by constructing filters sensitive to the edges of vessels having specific directions.

In order to emphasise the borders of vessels orthogonal to the direction of a given unit vector  $\mathbf{n}$  we use a regularised estimate of the directional derivative  $I_{\mathbf{n}}(\mathbf{x})$  of the original image  $I(\mathbf{x})$  in such a direction:

$$I_{\mathbf{n}}(\mathbf{x}) = \frac{dI(\mathbf{x})}{d\mathbf{n}} \approx \frac{dS(\mathbf{x})}{d\mathbf{n}} = \frac{d(G(\mathbf{x}) * I(\mathbf{x}))}{d\mathbf{n}} = G_{\mathbf{n}}(\mathbf{x}) * I(\mathbf{x})$$

where  $G_{\mathbf{n}}(\mathbf{x}) = \frac{dG(\mathbf{x})}{d\mathbf{n}}$  is a directional-derivative-of-Gaussian kernel (Figure 2 shows a plot of  $G_{\mathbf{n}}(\mathbf{x})$  for  $\mathbf{n} = [1, 0]$ ) and the last equation is due to the linearity of convolution and differentiation. The reason for using this approximation is that directional-derivative-of-Gaussian kernels can be decomposed as

$$G_{\mathbf{n}}(\mathbf{x}) = \mathbf{n} \cdot \nabla G(\mathbf{x}) = n_1 \frac{\partial G(\mathbf{x})}{\partial x_1} + n_2 \frac{\partial G(\mathbf{x})}{\partial x_2}$$

where  $n_1$  and  $n_2$  are the components of  $\mathbf{n}$ . This means that  $I_{\mathbf{n}}(\mathbf{x})$  can be obtained at the cost of one addition and two multiplications per pixel once  $\frac{\partial G(\mathbf{x})}{\partial x_i} * I(\mathbf{x})$  (for  $i = 1, 2$ ) are known. Fortunately, such convolutions are not required at all as partial-derivatives-of-Gaussian masks can be decomposed further with considerable accuracy by means of properly shifted Gaussian kernels [5, 19, 26]. For example,

$$\frac{\partial G(\mathbf{x})}{\partial x_1} \approx \frac{1}{\sigma} \left[ G\left(\mathbf{x} + \left(\frac{\sigma}{2}, 0\right)\right) - G\left(\mathbf{x} - \left(\frac{\sigma}{2}, 0\right)\right) \right].$$

Therefore  $\frac{\partial G(\mathbf{x})}{\partial x_i} * I(\mathbf{x})$  can be estimated from  $S(\mathbf{x})$  at the cost of one subtraction and one multiplication per pixel only.

### 4.4 Directional Vessel Enhancement

By combining properly shifted versions of our efficient realisation of  $G_{\mathbf{n}}(\mathbf{x})$  it is now possible to build efficient filters sensitive to vessel-like structures in any given direction.

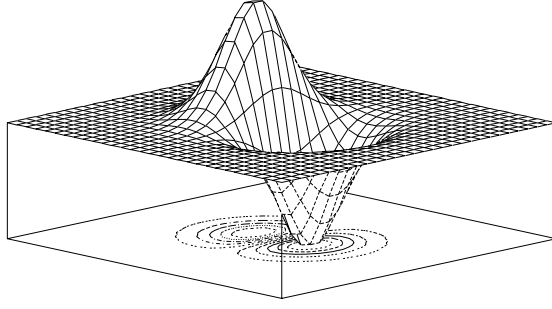


Figure 2: Plot of a directional-derivative-of-Gaussian operator  $G_{\mathbf{n}}(\mathbf{x})$ .

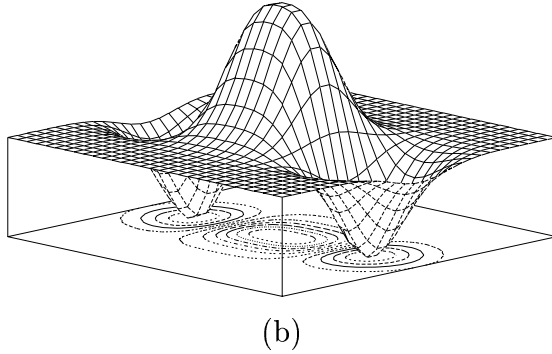
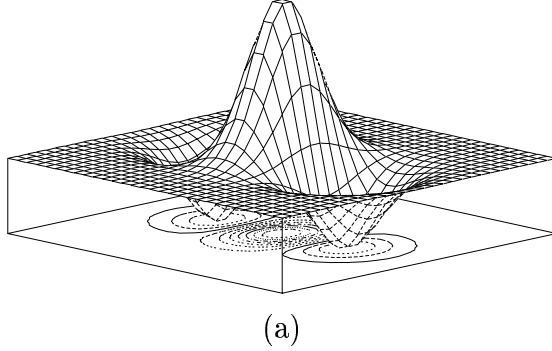


Figure 3: Kernels  $B_{\mathbf{n}}(\mathbf{x}, w)$  with half-width  $w = \sigma$  (a) and  $w = 2\sigma$  (b).

The simplest of such filters, shown in Figures 3(a)–(b), is:

$$B_{\mathbf{n}}(\mathbf{x}, w) = G_{\mathbf{n}}(\mathbf{x} + w\mathbf{n}) - G_{\mathbf{n}}(\mathbf{x} - w\mathbf{n}).$$

It is easy to convince one-selves that, for values of  $w$  not too large with respect to  $\sigma$ ,  $B_{\mathbf{n}}(\mathbf{x}, w)$  is actually a vessel detector by considering that only vessel-like structures of appropriate thickness and direction can overlap with the central positive area without touching the negative side lobes. This is also corroborated the fact that shape of such a kernel resembles that of the optimum ridge and roof detectors suggested by Canny [7, 8].

In order to increase the directional selectivity of the filter, we can use a combination of two or more kernels  $B_{\mathbf{n}}(\mathbf{x}, w)$ . For example we can use the following composition of  $2N + 1$  properly shifted kernels:

$$\bar{B}_{\mathbf{n}}(\mathbf{x}, w, l) = \frac{1}{2N + 1} \sum_{k=-N}^N B_{\mathbf{n}}(\mathbf{x} + l \frac{k}{N} \mathbf{t}, w)$$

where  $\mathbf{t}$  is a unit vector orthogonal to  $\mathbf{n}$  and  $l$  is the half-length of the resulting kernel.

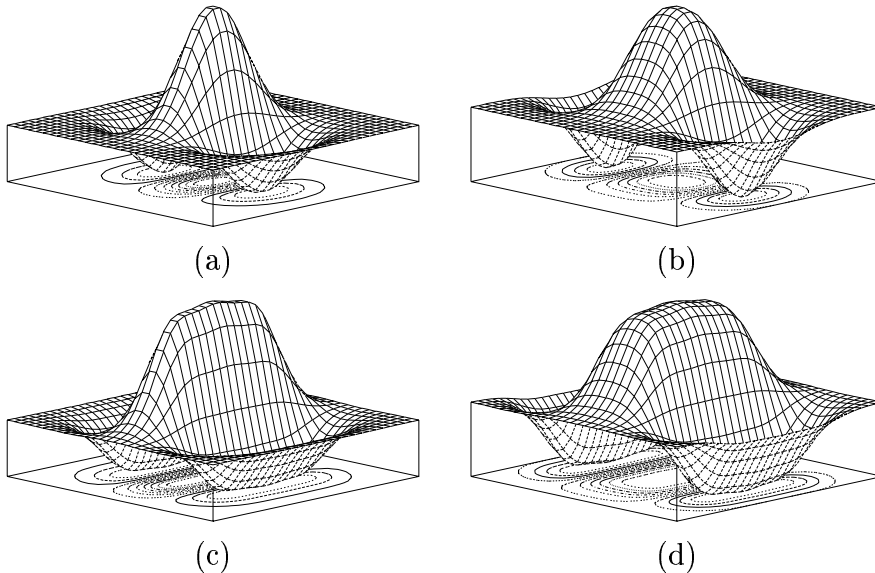


Figure 4: Directional kernels  $\bar{B}_{\mathbf{n}}(\mathbf{x}, w, l)$  in the following cases: (a) half-length  $l = \sigma$  and half-width  $w = \sigma$ , (b)  $l = \sigma$  and  $w = 2\sigma$ , (c)  $l = 2\sigma$  and  $w = \sigma$ , (d)  $l = 2\sigma$  and  $w = 2\sigma$ .

Figures 4(a)–(d) show the plots of  $\bar{B}_{\mathbf{n}}(\mathbf{x}, w, l)$  for different combinations of  $w$  and  $l$  in the case of  $N = 1$ . It is apparent that for any fixed  $w$  and  $l$  the directional selectivity of this kernel is considerably higher than that of  $B_{\mathbf{n}}(\mathbf{x}, w)$ .<sup>3</sup>

It should be noted that the kernels shown in Figures 4(a)–(d) are similar to the receptive fields of simple cells in the visual cortex [21], to the filters designed by Zucker for tangent field estimation in textured images [40], to those designed by Malik and Perona for finding boundaries generated by texture or gray-level discontinuities [26] and to some Gabor functions [14]. Unfortunately, this similarity means that they share a common unwanted (in our case) behaviour: they tend to respond also in the presence of step edges. In the next section we will see how to prevent this.

## 4.5 Directional Filter Integration and Validation

In order to obtain an image in which blood vessels are enhanced independently of their direction and width, it is necessary to integrate the images produced by convolution with kernels  $\bar{B}_{\mathbf{n}}(\mathbf{x}, w, l)$  of different orientation, half-width and half-length, into a single enhanced image. The integration can be performed on the ground of the following considerations.

By design, each filter is specialised in enhancing all vessels having a given width and orientation and attenuating every other structure. For any given pixel in the image there will be a directional filter that gives a maximum output. If such a pixel belongs to a non-vessel-like structure, the filter which responds maximally will give a small output, like all the other filters. Therefore, in this situation, considering the output of such a filter as the overall output of the vessel enhancement algorithm instead of, for instance, a combination of the outputs of all the filters does not make any significant difference. If, on the contrary, the considered pixel belongs to a vessel or an elongated background pattern, such a structure must have exactly the same orientation and width of the filter

<sup>3</sup>This fact can also be easily checked by comparing the output images produced by convolving the test image in Figure 5(a) with  $B_{\mathbf{n}}(\mathbf{x}, w)$  and  $\bar{B}_{\mathbf{n}}(\mathbf{x}, w, l)$ .

which responds maximally (otherwise another filter would have given a bigger response). Therefore, the output of such a filter gives a measure of how similar to a vessel is the structure around the given pixel. If the output of the enhancement algorithms has to be used by a vessel detection algorithm, such a similarity measure is the most appropriate overall output to make a decision on whether the pixel belongs to a vessel or not. These considerations alone would lead to the following integration formula:

$$\mathcal{E}(\mathbf{x}) = \max_{\mathbf{n}, w, l} \bar{B}_{\mathbf{n}}(\mathbf{x}, w, l) * I(\mathbf{x}).$$

The compound output  $\mathcal{E}(\mathbf{x})$  is maximum in the presence of light vessels on a dark background (the opposite behaviour can be easily obtained by appropriate sign changes). However, as the directional filters  $\bar{B}_{\mathbf{n}}(\mathbf{x}, w, l)$  tend to respond also in the presence of step edges, such structures tend to be present in  $\mathcal{E}(\mathbf{x})$ .

To prevent this, it is necessary to validate the output of the directional filters before integration by checking whether the gray level of the central pixel of  $\bar{B}_{\mathbf{n}}(\mathbf{x}, w, l)$  is greater than the gray levels of the pixels laying on the “left” and “right” with respect to a direction orthogonal to  $\mathbf{n}$ . More formally, we can define the validated directional enhanced image  $V_{\mathbf{n}}(\mathbf{x}, w, l, v)$  as:

$$V_{\mathbf{n}}(\mathbf{x}, w, l, v) = \begin{cases} \bar{B}_{\mathbf{n}}(\mathbf{x}, w, l) * I(\mathbf{x}) & \text{if } S(\mathbf{x} + v\mathbf{n}) < S(\mathbf{x}) \text{ and} \\ & S(\mathbf{x} - v\mathbf{n}) < S(\mathbf{x}), \\ 0 & \text{otherwise.} \end{cases}$$

In such a definition, validation is performed by comparing the gray levels of just three pixels. Larger sets of pixels could be used if a more robust validation were needed.

Once the validated directional images are available for different directions, half-widths and half-lengths, they can be integrated to construct a single validated image

$$\mathcal{V}(\mathbf{x}, v) = \max_{\mathbf{n}, w, l} V_{\mathbf{n}}(\mathbf{x}, w, l, v).$$

It should be noted that the integration of the output of filters with different  $w$  is required only if directional filters with a single width are not capable of enhancing vessels of all possible widths of interest in the particular problem at hand. However, as will be shown in Section 5, this is seldom the case as our directional filters are sensitive to bars of different widths, up to values several times  $\sigma$ . Similarly, the integration of the output of filters with different half-lengths is often unnecessary when small values of  $l$  are adopted.

In general, the value of the distance  $v$  used for validation should be greater than the half-width of the largest structures of interest. A useful exception to this rule is validation with  $v = 1$ . In this case directional filters with validation behave as directional local-maxima detectors. This means that the validated image  $\mathcal{V}(\mathbf{x}, 1)$  is a representation in which the ridges of the bar-like structures contained in the original image, i.e. the skeletons of the vessels, are highly enhanced (like in [17, 29]).

## 4.6 Vessel Detection and Segmentation

As the validated integrated output  $\mathcal{V}(\mathbf{x}, v)$  is computed by using only a few operations per pixel, the enhancement algorithm described above can be used to improve the performance of virtually any sophisticated vessel detection/segmentation technique without changing significantly to the computation load associated with it. However, when the intensity of structural and non-structural noise is not too high, the validated images

obtained with  $v = 1$  and with  $v$  larger than the half-width of the thickest vessel of interest can be used in conjunction with simple detection algorithms for the near-realtime extraction of vessel skeletons and for the segmentation of vessels, respectively.

For instance, it is possible to adopt a fast but robust technique known as *thresholding with hysteresis* [8] whose only assumption is the connectedness of vessels. The algorithm requires that two thresholds be predefined:  $T_{low}$  and  $T_{high}$ . Each pixel of the validated image whose gray level  $\mathcal{V}(\mathbf{x}, v)$  is higher than  $T_{high}$  is considered as a *seed pixel*. Segmentation is obtained by taking all the pixels for which  $\mathcal{V}(\mathbf{x}, v) \geq T_{low}$  and that are connected to a seed pixel directly or via other pixels having  $\mathcal{V}(\mathbf{x}, v) \geq T_{low}$ . To make the algorithm independent of imaging-chain parameters (e.g. the gain of the video camera)  $T_{low}$  and  $T_{high}$  are selected so that  $Prob \{ \mathcal{V}(\mathbf{x}, v) \geq T_{low} \} = p_{low}$  and  $Prob \{ \mathcal{V}(\mathbf{x}, v) \geq T_{high} \} = p_{high}$ , with  $p_{low}$  and  $p_{high}$  prefixed constants.

## 5 Parameter Selection

The most adequate set of parameters for our vessel enhancing strategy depends on several things: the characteristics of noise, the digitisation parameters, the width of the thickest and thinnest vessels of interest, the tortuosity of the vessels in the imaged anatomical district, their predominant orientation, etc. Therefore, given a particular application some experiments are required to choose the best parameters. However, as the enhancement and detection algorithms described in the previous sections are very efficient and include only a small number of parameters, several effective strategies are available for the optimisation of their values.

The first strategy is to define a quality criterion, based for example on the comparison between the output of our algorithm and a set of otherwise-enhanced or hand-segmented images, and use a numeric optimisation technique (e.g. a genetic algorithm) to discover the best set of parameters. In most cases even the brute force approach of sampling the whole parameter space can work because most parameters can have only two or three meaningful values, while the others can be coarsely discretised.

An alternative to this is “visual” optimisation, i.e. to apply the algorithms with different parameters to a set of images, look at them, “get a feel” for how each parameter influences the results and then select a set of parameters that give the best visual quality. To show how this can be done and illustrate the influence of each parameter, in this section we report on experiments performed on two  $256 \times 256$ , 8-bit synthetic images of bar-like patterns of different width and orientation and hand-drawn vessel-like structures with additive noise of high intensity.

The first test image, shown in Figure 5(a), includes 10 concentric rings having different widths and smooth borders. It has been obtained by sampling the radial function

$$f(\mathbf{x}) = \begin{cases} k_a \left( 1 + \cos(k_f \frac{\|\mathbf{x}-\mathbf{x}_0\|^2}{k_h}) \right) & \text{if } \|\mathbf{x} - \mathbf{x}_0\|^2 \in [k_l, k_h] \\ 0 & \text{otherwise,} \end{cases}$$

with the following parameters:  $\mathbf{x}_0 = (127.5, 127.5)$ ,  $k_l = 9.1125 \times 10^4$ ,  $k_h = 1.728 \times 10^6$ ,  $k_a = 127.5$  and  $k_f = 21\pi$ . The second test image, shown in Figure 5(b), includes vessel-like structures of different thickness on a dark background. The image, which vaguely resembles a projection of the left coronary artery, has been obtained by successively hand-drawing and smoothing vessels of smaller and smaller thickness. To make the image more realistic and to show the noise-rejection capabilities of the filters, uniform noise with a variance of 1000 has been added to it. Figure 5(c) shows the resulting test image.

## Influence of the Number of Directional Filters

The first test image can be used to show the effect of varying the number of directional filters considered in generating the output of the enhancement algorithm. Figure 6(a) shows the output  $\mathcal{E}(\mathbf{x})$  of a vessel enhancing filter with parameters  $\sigma = 1$ ,  $N = 1$ ,  $l = 2$  and  $w = 1$  when only two orthogonal directions,  $\mathbf{n} = (1, 0)$  and  $\mathbf{n} = (0, 1)$ , are used (a constant gray level has been added to the image to allow for the display of both positive and negative output values). Figure 6(b) shows the output of the same filter when two more directions,  $\mathbf{n} = (1/\sqrt{2}, 1/\sqrt{2})$  and  $\mathbf{n} = (1/\sqrt{2}, -1/\sqrt{2})$ , are considered.

It can be noted that, in both cases, filters designed to enhance very thin bar-like structures are actually sensitive to bars of many different scales. In fact, the amplitude of the output of the filters decreases significantly only in the presence of the two thickest rings. In addition, it can be noted that while the integration of the output of two directional filters does not provide sufficient directional isotropy, the image obtained with four directional filters is nearly rotation-invariant.

To investigate the influence of the other parameters of the algorithm, in the following experiments we have used the second test image which contains vessels in nearly all directions. Therefore, we have decided to adopt four directional filters. However, when vessels are expected to have certain directions only, much more efficient algorithms can be obtained by choosing one or two properly oriented directional filters.

## Influence of $\sigma$

Figure 7 shows the enhanced images obtained with different values of the standard deviation  $\sigma$  of the Gaussian kernel  $G(\mathbf{x})$ ,  $l = 2\sigma$  and  $w = \sigma$ . It is apparent that the choice  $\sigma = 1$  provides crisper images with better defined vessel-boundaries (even though the thickest vessels tend to be thinned). Thanks to the integration of four selective directional filters, noise rejection is already rather good for such a small value of  $\sigma$ . Filters with a larger  $\sigma$  have better noise rejection capabilities but do not seem sensitive enough to the smallest vessels in the image. Therefore,  $\sigma = 1$  seems the best trade-off for this image. Images where vessels differ significantly in size with respect to the ones present in this test image will probably require a different trade-off value for  $\sigma$ .

## Influence of $w$

The effect of varying the half-width  $w$  of directional kernels is illustrated in Figure 8. Vessels appear well defined and enhanced both for  $w = 1$  and for  $w = 2$ . However, the larger kernel has a stronger noise rejection and a better response in the presence of thick vessels. A disadvantage of such a kernel is a slight blurring of the thinnest vessels. The best compromise seems to be  $w = 2$  in this case.

## Influence of $l$

The effect of varying the half-length  $l$  of directional kernels is illustrated in Figure 9. Disregarding noise, the structural differences among the output images do not seem significant. Only for  $l = 3$  a slight rotational variance and an attenuation of the output around bifurcations seem to be present. However, as noise rejection is clearly an increasing function of  $l$ , relatively large values of half-length seem a better choice. (Note that  $\bar{B}_{\mathbf{n}}(\mathbf{x}, w, 0) \equiv B_{\mathbf{n}}(\mathbf{x}, w)$ .) Therefore, the best trade-off in this case is  $l = 2$ .

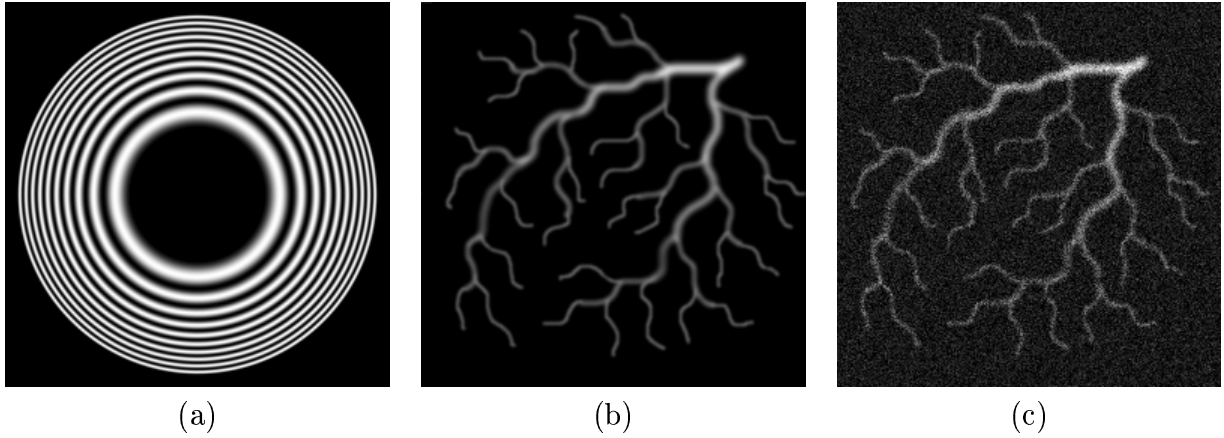


Figure 5: Synthetic test image of concentric rings of different widths (a), and hand-drawn images of vessel-like structures without (b) and with (c) additive noise.

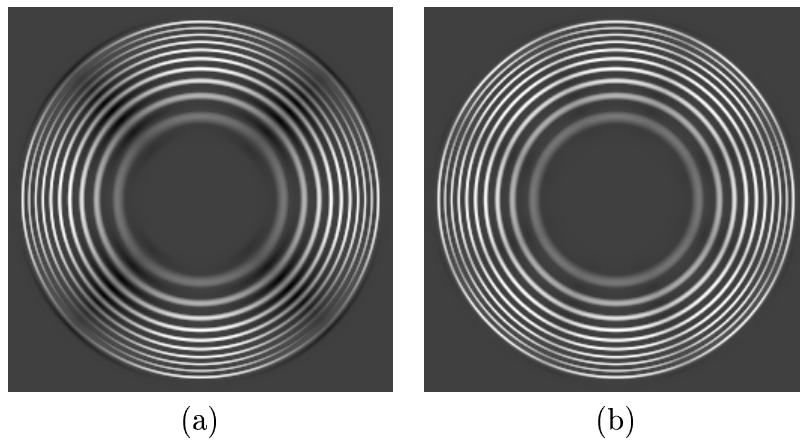


Figure 6: Output  $\mathcal{E}(\mathbf{x})$  obtained with vessel enhancing filters with parameters  $l = 2$  and  $w = 1$  when two (a) and four (b) different directions  $\mathbf{n}$  are considered.

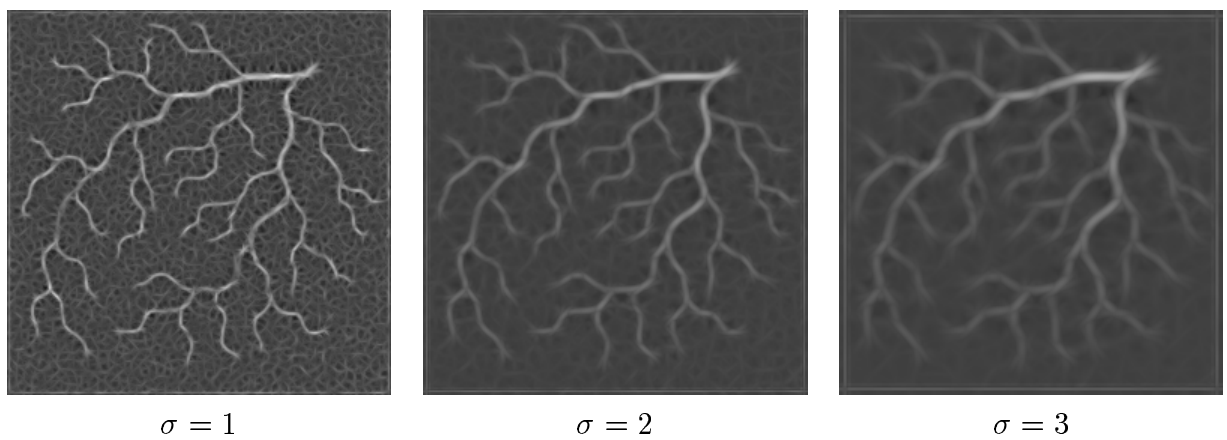


Figure 7: Output  $\mathcal{E}(\mathbf{x})$  produced by vessel enhancing filters with parameters  $l = 2\sigma$  and  $w = \sigma$  with  $\sigma = 1, 2, 3$  when applied to the image in Figure 5(c).

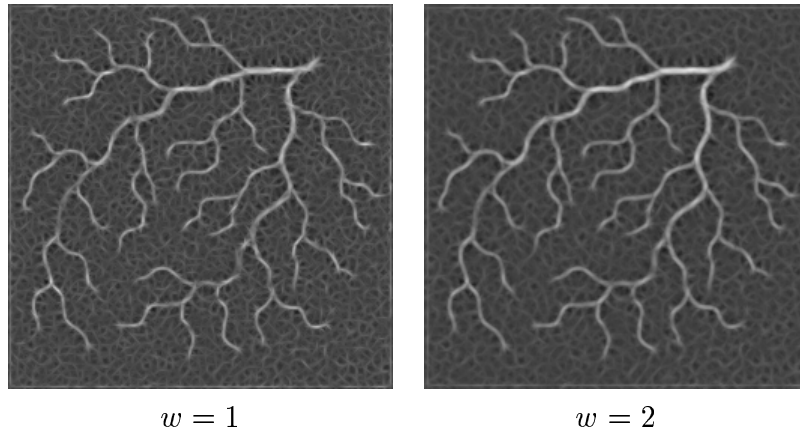


Figure 8: Output  $\mathcal{E}(\mathbf{x})$  produced by vessel enhancing filters with parameters  $\sigma = 1$  and  $l = 2$  with  $w = 1, 2$  when applied to the image in Figure 5(c).

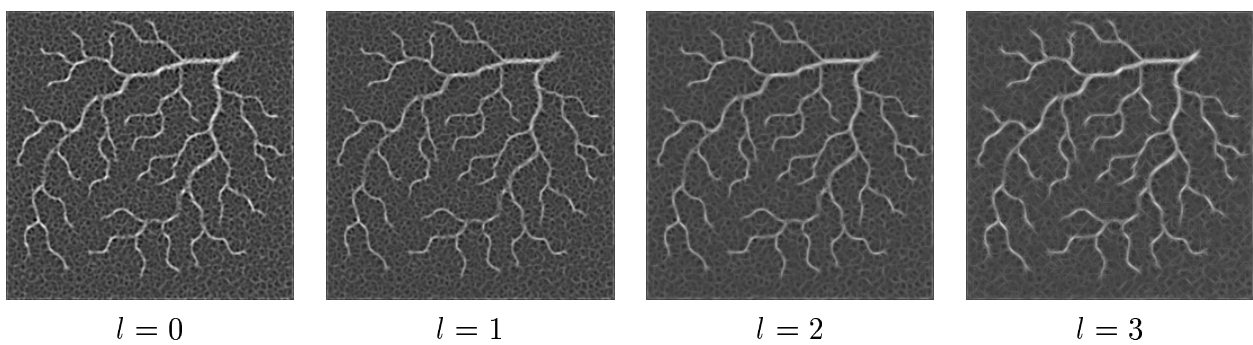


Figure 9: Output  $\mathcal{E}(\mathbf{x})$  produced by vessel enhancing filters with parameters  $\sigma = 1$  and  $w = 1$  with  $l = 0, 1, 2, 3$  when applied to the image in Figure 5(c).

## Effect of Multi-Width Integration

Figure 10 illustrates the effect of integrating the output of filters with different half-widths  $w$ . In the image that results from the integration of the output of four directional filters with  $w = 1$  and four with  $w = 2$ , both thin and thick vessels appear well defined and enhanced. This is a better result than the one obtained with any single  $w$ . Obviously, due to the max operator, also the noise affecting the background is “integrated”. However, it does not seem much different from the noise present in  $\mathcal{E}(\mathbf{x})$  when only filters with  $w = 1$  are used.

## Effect of Validation

The effect of validation is shown in Figure 11. Actually, as suggested in Section 4, when  $v = 1$ , filtering with validation is a kind of ridge enhancement or vessel skeletonizing. As  $v$  increases the skeletons seem to become thicker and thicker until the real size of each vessel is reached. Positive effects of validation are the zeroing of negative areas present in the non-validated output near vessel borders, and a considerable noise reduction. A possibly negative effect is that thin vessels that originate from thick vessels can be zeroed near bifurcations. However, the advantages of validation seem to prevail with respect to the disadvantages.

## Skeleton Detection and Vessel Segmentation

The results of applying the method of hysteresis thresholding to validated images are illustrated in Figure 12. For the sake of brevity, only the results with best sets of parameters are shown: for the segmentation of the validated image obtained with  $v = 6$  they are  $p_{low} = 0.10$  and  $p_{high} = 0.03$ , for the skeleton-enhanced image smaller probability values,  $p_{low} = 0.05$  and  $p_{high} = 0.02$ , are more appropriate as fewer pixels represent vessel skeletons.

# 6 Experimental Results

In order to show the robustness and sensitivity of the vessel enhancement and detection approach described in Section 4 in the presence of real, noisy images of blood vessels, in this section we report on experiments performed with left and right coronary angiograms of different patients. The images had a spatial resolution of  $256 \times 256$  pixels and a intensity resolution of 256 gray-levels.

Figures 13 and 14 illustrates the results obtained with eight patients. As shown in rows (a), the original images have different contrast and include a considerable amount of noise and unwanted structures (ribs, diaphragm muscle, metallic plates, borders of the image intensifier, etc.).

Rows (b) report the images  $\mathcal{E}(\mathbf{x})$  produced by integrating the output of four directional filters with parameters  $\sigma = 1$ ,  $w = 2$ ,  $N = 1$  and  $l = 2$ . Even if, in such images, a large part of the structural and non-structural noise has been suppressed, elongated patterns due to noise as well as the borders of the ribs, the diaphragm, the image intensifier, etc. are still present. The computation of each of these enhanced images has required 22 additions/subtractions and 5 multiplications/shifts (for directional filtering) plus 3 comparisons (for integration) per pixel.

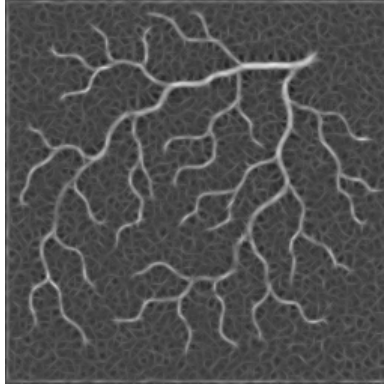


Figure 10: Image obtained by integrating by output produced by vessel enhancing filters with parameters  $\sigma = 1$ ,  $l = 2$  and  $w = 1, 2$  applied to the image in Figures 5(c).

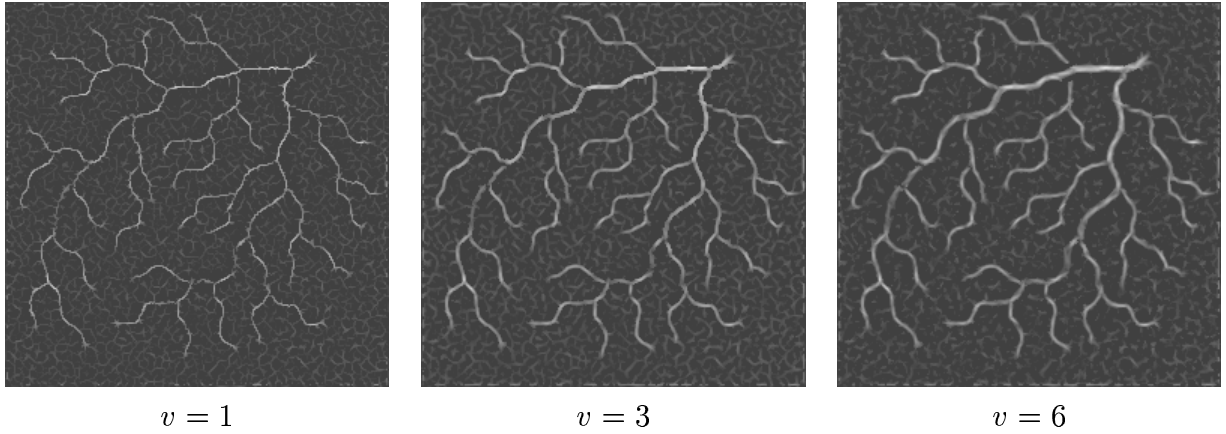


Figure 11: Validated output  $\mathcal{V}(\mathbf{x}, v)$  produced by vessel enhancing filters with parameters  $\sigma = 1$ ,  $w = 1$ ,  $l = 2$  with  $v = 1, 3, 6$  when applied to the image in Figure 5(c).

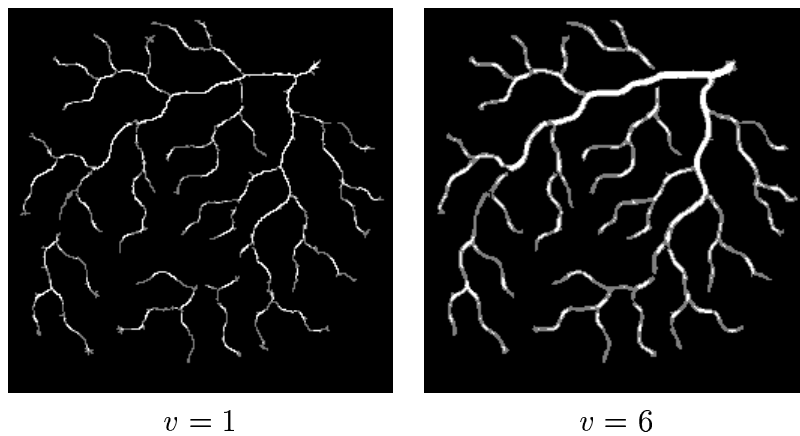


Figure 12: Results of hysteresis thresholding of validated images with parameters  $\sigma = 1$ ,  $l = 2$ ,  $w = 2$  with  $v = 1, 6$  obtained from the image in Figure 5(c). Seed pixels ( $\mathcal{V}(\mathbf{x}, v) \geq T_{high}$ ) are drawn in white; pixels with  $\mathcal{V}(\mathbf{x}, v) \geq T_{low}$  connected to seed pixels are drawn in gray.

Validated images  $\mathcal{V}(\mathbf{x}, 6)$  and  $\mathcal{V}(\mathbf{x}, 1)$  are shown in rows (c) and (d), respectively. At least two positive effects of validation can be noted: i) most of the borders produced by structures different from vessels have been suppressed, ii) noise has been considerably reduced. The computation of each validated image has required the same operations needed for directional filtering plus 8 comparisons per pixel (for validation).

Rows (e) and (f) illustrate the results of applying thresholding with hysteresis to validated images. Probability values  $p_{low} = 0.10$  and  $p_{high} = 0.03$  have been used for images validated with  $v = 6$ , while  $p_{low} = 0.06$  and  $p_{high} = 0.015$  have been adopted for  $v = 1$ . Despite the fact that a considerable amount of noise is present in the input images and that no linearization has been performed, the segmentation and the skeletons of vessels produced with such a simple procedure seem quite good. In particular, most of the thickest and many thinner vessels are represented and only a few false detections are present.<sup>4</sup>

## 7 Final Remarks

In this paper we have presented an algorithm for the enhancement and detection of blood vessels in medical images which has been designed according to a rather unusual approach: to achieve the maximum quality of result in real- or near real-time.

The reduced number of operations per pixel required, most of which being additions or comparisons, allows us to qualify our vessel-enhancement strategy as highly efficient. With a minimum approximation, all the operations involved in the algorithm can be performed in integer arithmetics. This feature has allowed us to obtain very fast implementations also on general purpose workstations. For example, a DEC Alpha 300MHz computer can enhance with validation a  $256 \times 256$  image in 77.1ms (approximately corresponding to a rate of 13 images per second). This suggests that an implementation based on the hardware operations available in many image processing boards could allow for on-line, video-rate vessel enhancement and detection.

Experimental results with synthetic and real images have shown the considerable noise rejection capability of the algorithm and its very good sensitivity to vessels. Obviously, having designed the algorithm not to disfavour efficiency in favour of quality we cannot claim that the quality of the results it produces is superior to those of other algorithms present in the literature. What we can claim is that it offers one of the highest quality/computation ratios.

## 8 Acknowledgements

This work was partially supported by the grants of the Italian Ministry of University and Scientific and Technologic Research (MURST), the Italian National Research Council (CNR) and the British Council-MURST/CRUI programme.

---

<sup>4</sup>In should be noted that applied to non-subtracted coronarographic images even the most sophisticated vessel-segmentation algorithms can seldom extract more than 80% of the pixels belonging to vessels and produce less then 5% false detections.

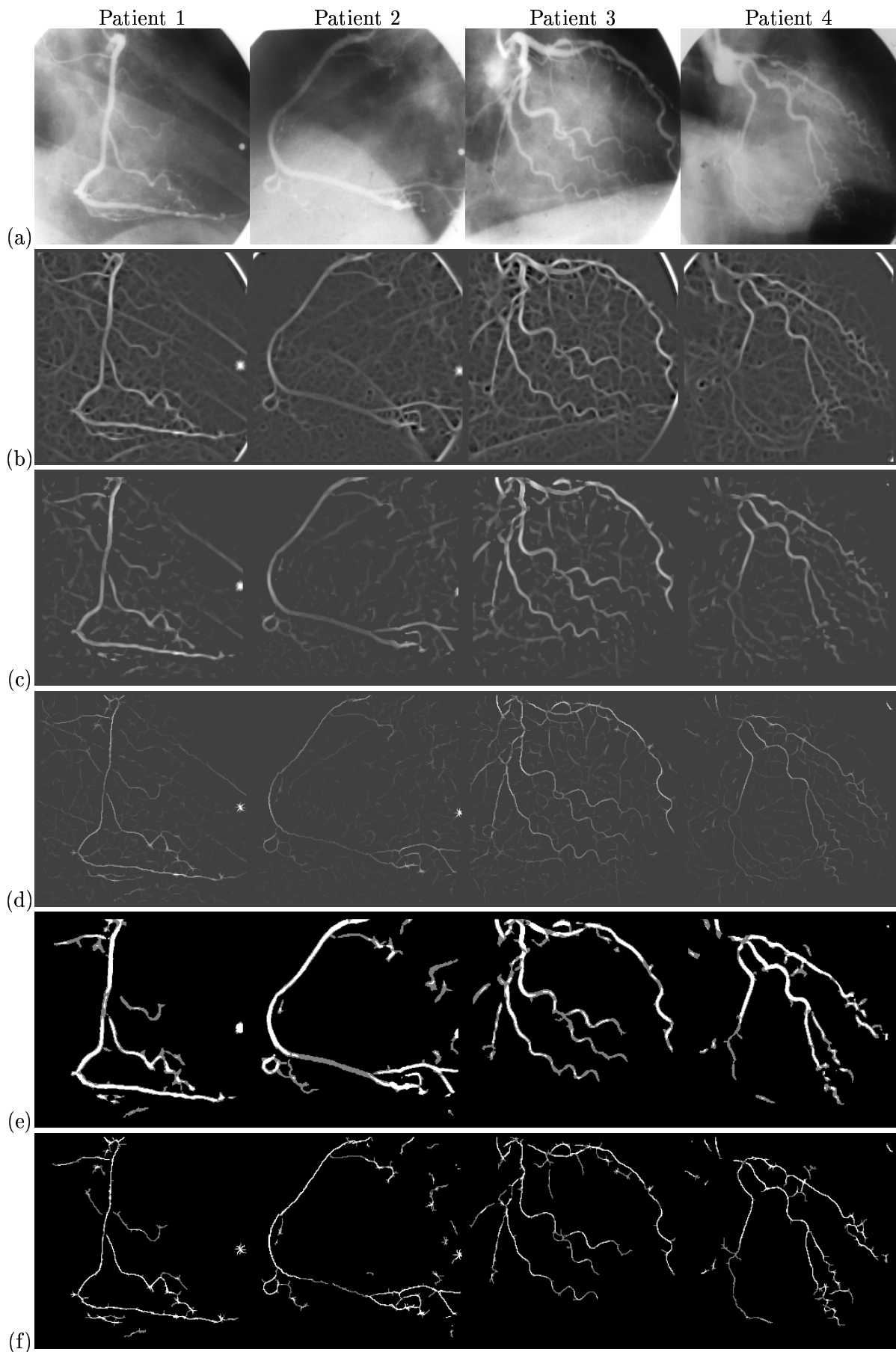


Figure 13: Vessel enhancement and detection on real coronary angiograms: (a) original images, (b) enhanced images  $\mathcal{E}(\mathbf{x})$ , (c) validated images  $\mathcal{V}(\mathbf{x}, 6)$ , (d) validated images  $\mathcal{V}(\mathbf{x}, 1)$ , (e) hysteresis thresholding of  $\mathcal{V}(\mathbf{x}, 6)$ , and (f) hysteresis thresholding of  $\mathcal{V}(\mathbf{x}, 1)$ .

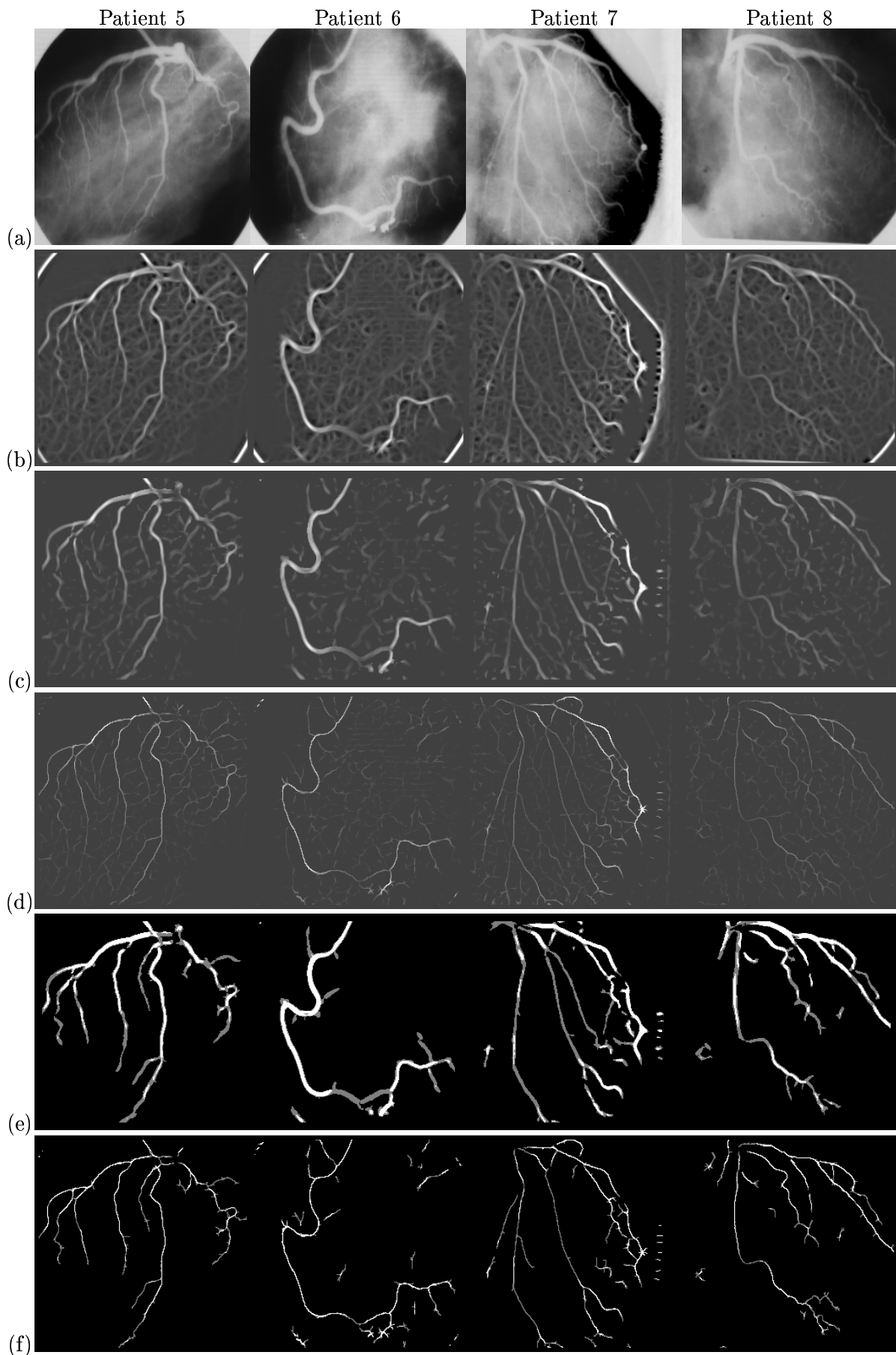


Figure 14: Vessel enhancement and detection on real coronary angiograms: (a) original images, (b) enhanced images  $\mathcal{E}(\mathbf{x})$ , (c) validated images  $\mathcal{V}(\mathbf{x}, 6)$ , (d) validated images  $\mathcal{V}(\mathbf{x}, 1)$ , (e) hysteresis thresholding of  $\mathcal{V}(\mathbf{x}, 6)$ , and (f) hysteresis thresholding of  $\mathcal{V}(\mathbf{x}, 1)$ .

## References

- [1] N. Alperin, K. R. Hoffmann, K. Doi, and K. G. Chua, Automated analysis of coronary lesions from cineangiograms using vessel tracking and iterative deconvolution techniques, in *Proceedings of Computers in Cardiology*, pp. 153–156 (IEEE Computer Society Press, Jerusalem, 1990).
- [2] S. M. Astley and J. N. H. Brunt, Exploitation of computer vision technology in coronary cineangiographic analysis, in *Proceedings of Computers in Cardiology*, pp. 579–582 (IEEE Computer Society Press, 1987).
- [3] R. Aufrichtig, D. Geiger, A. Singh, and D. L. Wilson, Spatio-temporal X-ray fluoroscopy filtering using object detection, in *Proceedings of Computers in Cardiology*, pp. 587–590, (IEEE Computer Society Press, London, 1993).
- [4] K. Barth, B. Eicker, R. Kock, and P. Marhoff, Automated three-dimensional recognition of the coronary tree with clinical DSA image pairs, in *Proceedings of Computers in Cardiology*, pp. 187–189 (IEEE Computer Society Press, 1988).
- [5] J. Ben-Arie, Multi-dimensional linear lattice for Fourier and Gabor transforms, multiple-scale Gaussian filtering, and edge detection, in *Neural Networks for Perception, Vol. 1*, ed. Harry Wechsler, pp. 214–233 (Academic Press, San Diego, CA, 1992).
- [6] R. Calamai, G. Coppini, M. Demi, R. Poli, and G. Valli, A computational approach to medical imaging, *Journal of Nuclear Medicine and Allied Sciences*, 34/1 (1990) 42–50.
- [7] J. F. Canny, A computational approach to edge detection, *IEEE Transactions on Pattern Analysis and Machine Intelligence*, 8/6 (1986) 679–698.
- [8] J. F. Canny, Finding edges and lines in images, Technical Report 720, Artificial Intelligence Laboratory, Massachusetts Institute of Technology, June 1983.
- [9] J.Y. Catros and D. Mischeler, An artificial intelligence approach for medical picture analysis, *Pattern Recognition Letters*, 8 (1988) 123–130.
- [10] S. Chaudhuri, S. Chatterjee, N. Katz, M. Nelson, and M. Goldbaum, Detection of blood vessels in retinal images using two-dimensional matched filters, *IEEE Transactions on Medical Imaging*, 8/3 (1989) 263–269.
- [11] J.S. Chen, A. Huertas, and G. Medioni, Fast convolution with Laplacian-of-Gaussian masks, *IEEE Transactions on Pattern Analysis and Machine Intelligence*, 8 (1987) 584–590.
- [12] G. Coppini, M. Demi, R. Poli, and G. Valli, An artificial vision system for X-ray images of human coronary trees, *IEEE Transactions on Pattern Analysis and Machine Intelligence*, 15/2 (1993) 156–162.
- [13] P.-E. Danielsson and O. Seger, Generalized and separable Sobel operators, in *Machine vision for three-dimensional scenes*, ed. Herbert Freeman, pp. 347–379 (Academic Press, Boston, 1990).

- [14] J. G. Daugman, Complete discrete 2-D Gabor transforms by neural networks for image analysis and compression, *IEEE Transactions on Acoustics, Speech and Signal Processing*, 36/7 (1988) 1169–1179.
- [15] P.H. Eichel, E.J. Delp, K. Koral, and A.J Buda, A method for a fully automatic definition of coronary arterial edges from cineangiograms, *IEEE Transactions on Medical Imaging*, 7 (1988) 313–320.
- [16] J. L. Elion, A knowledge-based expert system for the automated identification of structures in coronary angiograms, in *Computers in Cardiology*, pp. 201–204, (IEEE Computer Society Press, 1988).
- [17] M. A. Fischler and H. C. Wolf, Linear delineation, in *Proc. IEEE Conference on Computer Vision and Image Processing*, pp. 351–356 (Washington, D.C., June 19–23 1983).
- [18] S. R. Fleagle, M. R. Johnson, C. J. Wilbricht, D. J. Skorton, R. F. Wilson, C. W. White, M. L. Marcus, and S. M. Collins, Automated analysis of coronary arterial morphology in cineangiograms: Geometric and physiologic validation in humans, *IEEE Transactions on Medical Imaging*, 8/4 (1989) 387–400.
- [19] J. R. Fram and E. S. Deutsch, On the quantitative evaluation of edge detection schemes and their comparison with human performance, *IEEE Transactions on Computers*, 24/6 (1975) 616–628.
- [20] G. Gerig, th. Koller, G. Széleky, Ch. Brechbühler, and O. Kübler, Segmentation and symbolic description of cerebral vessel structure based on MR angiography volume data, in *Computer Assisted Radiology, CAR'93*, eds. H. U. Lemke, K. Inamura, C. C. Jaffe, and R. Felix, pp. 359–365 (Springer-Verlag, Berlin, 1993).
- [21] D. H. Hubel and T. N. Wiesel, Functional architecture of macaque monkey visual cortex, *Proceedings of the Royal Society of London (B)*, 198 (1977) 1–59.
- [22] K. Kitamura, J.M. Tobis, and J. Sklansky, Estimating the 3-D skeletons and transverse areas of coronary arteries from biplane angiograms, *IEEE Transactions on Medical Imaging*, 7 (1988) 173–187.
- [23] C. G. Kooijman, R. T. Rademaker, J. J. Gerbrands, and J. H. C. Reiber, Developments towards frame-to-frame computer processing of the entire coronary tree, in *Proceedings of Computers in Cardiology*, pp. 389–392 (IEEE Computer Society Press, 1983).
- [24] I. Liu and Y. Sun, Recursive tracking of vascular networks in angiograms based on the detection-deletion scheme, *IEEE Transactions on Medical Imaging*, 12/2 (1993) 334–341.
- [25] S. Lu and S. Eiho, Automatic detection of the coronary arterial contours with sub-branches from an X-ray angiogram, in *Proceedings of Computers in Cardiology*, pp. 575–578 (IEEE Computer Society Press, London, 1993).
- [26] J. Malik and P. Perona, Finding boundaries in images, in *Neural networks for perception, Vol. 1*, ed. Harry Wechsler, Chap. II.7, pp. 315–344 (Academic Press, 1992).

- [27] F. P. Miles and A. L. Nuttall, Matched filter estimation of serial blood vessels diameters from video images, *IEEE Transactions on Medical Imaging*, 12/2 (1993) 147–152.
- [28] R. Nekovei and Y. Sun, Backpropagation network and its configuration for blood-vessel detection in angiograms, *IEEE Transactions on Neural Networks*, 6/1 (1995) 64–72.
- [29] T. V. Nguyen and J. Sklansky, Computing the skeleton of coronary arteries in cineangiograms, *Computers and Biomedical Research*, 19 (1986) 428–444.
- [30] D. N. Smith, H. Colfer, J. F. Brymer, B. Pitt, and S. H. Kliman, A semiautomatic computer technique for processing coronary angiograms, in *Proceedings of Computers in Cardiology*, pp. 325–328 (IEEE Computer Society Press, 1982).
- [31] M. Sonka, C. J. Wilbricht, S. R. Fleagle, S. K. Tadikonda, M. D. Winniford, and S. M. Collins, Simultaneous detection of both coronary borders, *IEEE Transactions on Medical Imaging*, 12/3 (1993) 588–599.
- [32] M. R. Spiegel, *Probability and Statistics*, (McGraw-Hill, New York, 1975).
- [33] S. A. Stansfield, Angy: A rule-based expert system for automatic segmentation of coronary vessels from digital subtracted angiograms, *IEEE Transaction of Pattern Analysis and Machine Intelligence*, 8 (1986) 188–199.
- [34] Y. Sun, Automated identification of vessel contours in coronary arteriograms by an adaptive tracking algorithm. *IEEE Transactions on Medical Imaging*, 8 (1989) 78–88.
- [35] B. D. Thackray and A. C. Nelson, Semi-automatic segmentation of vascular network images using a rotating structuring element (ROSE) with mathematical morphology and dual feature thresholding, *IEEE Transactions on Medical Imaging*, 12/3 (1993) 385–392.
- [36] J. van Cleynenbreugel, F. Fierens, P. Suetens, and A. Oosterlinck, Knowledge-based improvement of automatic image interpretation for restricted scenes: two case studies, *Image and Vision Computing*, 6/4 (1988) 238–246.
- [37] H. Q. Wang, R. T. Ritchings, and A. C. F. Colchester, Image understanding system for carotid angiograms, *Image and Vision Computing*, 5/2 (1987) 79–83.
- [38] D. L. Wilson and C. Bertram, Morphological enhancement of coronary angiograms, in *Proceedings of Computers in Cardiology*, pp. 313–316 (IEEE Computer Society Press, Venice, 1991).
- [39] W. Xia and W. Lü, Correspondence analysis for regional tracking in coronary arteriograms, *IEEE Transactions on Medical Imaging*, 11/2 (1992) 153–160.
- [40] S. W. Zucker, Early orientation selection: tangent fields and the dimensionality of their support, *Computer Vision Graphics and Image Processing*, 32/1 (1985) 74–103.